

Dynamical decoupling based quantum sensing: Floquet spectroscopy

J. E. Lang,¹ R. B. Liu,² and T. S. Monteiro¹

¹*Department of Physics and Astronomy, University College London, Gower Street, London WC1E 6BT, United Kingdom*

²*Department of Physics, The Chinese University of Hong Kong, Hong Kong, China*

(Dated: March 4, 2022)

Sensing the internal dynamics of individual nuclear spins or clusters of nuclear spins has recently become possible by observing the coherence decay of a nearby electronic spin: the weak magnetic noise is amplified by a periodic, multi-pulse decoupling sequence. However, it remains challenging to robustly infer underlying atomic-scale structure from decoherence traces in all but the simplest cases. We introduce Floquet spectroscopy as a versatile paradigm for analysis of these experiments, and argue it offers a number of general advantages. In particular, this technique generalises to more complex situations, offering physical insight in regimes of many-body dynamics, strong coupling and pulses of finite duration. As there is no requirement for resonant driving, the proposed spectroscopic approach permits physical interpretation of striking, but overlooked, coherence decay features in terms of the form of the avoided crossings of the underlying quasienergy eigenspectrum. This is exemplified by a set of “diamond” shaped features arising for transverse-field scans in the case of single-spin sensing by NV-centers in diamond. We investigate also applications for donors in silicon showing that the resulting tunable interaction strengths offer highly promising future sensors.

PACS numbers:

I. INTRODUCTION

There is enormous interest in the rapidly advancing field of detection and imaging at the single spin level [1–4], mainly with NV colour centers but also other defects in diamond [5, 6] not only as a source of versatile qubits for quantum information [7–10] and entanglement generation [11], but principally because they underpin a new generation of quantum sensors, for magnetometry and atomic scale characterisation of the environment [12–18]. In the widely-studied case of dynamical decoupling quantum sensing, a sequence of pulses modulates the coherent evolution of the sensor and in some cases, sharp “dips” in coherence allow one to detect, and infer useful characteristics of, nearby single spins or small spin-clusters. Complexities in the environment being studied mean that the single isolated sharp dip is found in a restricted subset of the data and motivates the development of more general or alternative methods of analysis. In particular, many decoupling sequences are temporally periodic.

In this case, Floquet’s theorem provides a canonical form for the solution of periodically driven systems and has found wide applicability in various branches of quantum physics since 1965 [19], especially in light-matter interactions with continuous driving and multi-photon atomic physics. Floquet’s theorem can be applied to any periodic quantum Hamiltonian for which $\hat{H}(t + \tau_{tot}) = \hat{H}(t)$. In practical implementations, instead of analysing the eigenstates of the static Hamiltonian, which are appropriate only in the perturbative limit of weak driving, one employs instead the eigenspectrum of the one period time-evolution propagator. Floquet theory is employed in analysis also of Nuclear Magnetic Resonance (NMR) spectra and related [20], where applications are essentially limited to resonant and continuous driving.

But this approach has not been considered for analysis of coherence behaviors in this new generation of multipulse spin sensing experiments. We argue that the Floquet spectroscopy method proposed is better adapted to regimes of strong quan-

tum entanglement between the sensor and detected spin systems than signal processing methods applied to classical ac signals; or geometric approaches based on two-state systems. In this work, we find that Floquet theory can augment current methods of analysis in several ways:

(1) Floquet theory is equally applicable to off-resonant as to resonant driving. Understanding of spin-sensing data is often cast in signal processing terms: the multi-pulse sequence imposes a filter function which selects an ac signal with a reasonably well-defined characteristic frequency $\omega_{ac}/2\pi$ which may, in turn, be used to infer interatomic coupling parameters. When ω_{ac} is resonant with the pulse interval τ (see Fig. 1(c)), so when $\omega_{ac}/\pi = 1/(4\tau)$, a narrow dip in coherence is observed. Here we show that away from such resonances, or even for broadened resonances, Floquet theory can shed insight on other striking features which are not narrow dips but can, nevertheless, yield rich information for atomic scale characterisation. The key reason is that we show the widths and shapes of these features may be understood in terms of avoided crossings of an underlying Floquet spectrum.

(2) Current experiments operate primarily in regimes of weak-coupling. The pulses involve consecutive switching between two electronic states u, d ; the associated characteristic frequencies of the detected spins ω_u, ω_d can vary significantly, since, for stronger coupling, there is significant back-action and entanglement between the sensor and detected spins. For weak coupling, $\omega_u \simeq \omega_d$ and in addition average Hamiltonian theory models apply, predicting typically $\omega_{ac} \approx \frac{1}{2}(\omega_u + \omega_d)$. Floquet theory remains valid regardless of coupling strength; we examine regimes of failure, obtain alternative forms for ω_{ac} and show that the avoided crossings shed insight in these regimes. It remains also valid even if there is non-trivial evolution due to finite duration of the pulses, a problem only recently identified [17].

(3) For detection of two-state systems (spins or spin pairs which reduce to an effective pseudospin) geometric methods [16, 21] are widely used to interpret data and yield analytical

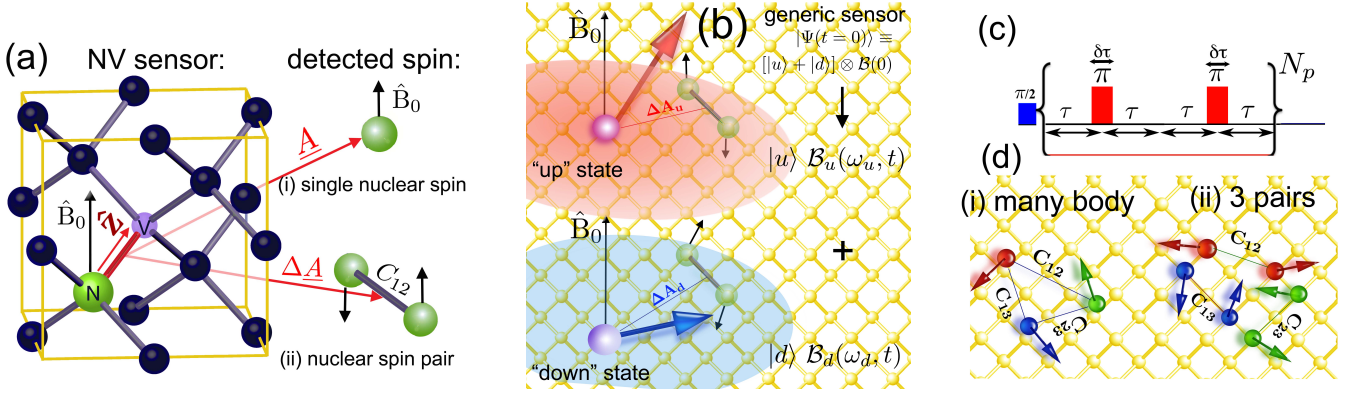


FIG. 1: (a) Current experiments have employed the $S = 1$ electronic spins of NV-centers to successfully detect (i) single nuclear spins [15, 21, 22] (ii) the internal dynamics of nuclear spin pairs [16] as well to characterise on the atomic scale, by estimating parameters such as electronic-nuclear dipolar couplings A and inter-nuclear dipolar couplings C_{12} . (b) Generic sensor detecting a pair of nuclear spins: the electronic spin state is in a superposition of “up” $|u\rangle$ and “down” $|d\rangle$ states. The nuclear dynamics and its characteristic frequencies $\omega_{u,d}$ depend on the electronic state. In turn, the electronic coherence is sensitive to the resulting weak ac noise from the nuclei. This may be amplified by dynamical decoupling control such as CPMG, leading to observed “dips” in coherence. These are at well-defined frequencies in typical weak coupling regimes where the nuclear dynamics is not too different in the u, d subspaces. However, strong coupling regimes do not necessarily yield sharp dips. (c) Additional complexities occur for pulses of finite durations (d) It is also challenging to differentiate between (i) independent pairs of spins and (ii) many-body effects from an equivalent interacting cluster. Floquet theory is not restricted to single spins or spin pairs and can be applied also to analysis of larger, correlated spin clusters, strong coupling and off-resonant driving.

expressions for the coherence decays. Although here the Floquet method already sheds additional physical insight, its full value is that it is universally valid even for higher dimensional state-spaces so would facilitate studies of e.g. multi-spin clusters.

The key-features of dynamical-decoupling based quantum sensing, using a multipulse periodic sequence, are illustrated in Fig.1. A $\pi/2$ pulse prepares the sensor system in a superposition state $\psi(t=0) = \frac{1}{\sqrt{2}}(|u\rangle + |d\rangle) \otimes \mathcal{B}(0)$, where $\mathcal{B}(0)$ is the detected spin-cluster at initial time. In turn, interaction with the sensor means that the spin-cluster becomes entangled with the sensor $\psi(t) \simeq \frac{1}{\sqrt{2}}(|u\rangle \mathcal{B}(\omega_u, t) + |d\rangle \mathcal{B}(\omega_d, t))$, where $\mathcal{B}(\omega_{u,d}, t) = (\hat{T}_{u,d})^{N_p} \mathcal{B}(0)$, for a pulse sequence (with propagator $\hat{T}_{u,d}$) which is repeated N_p times. The detected spin dynamics is associated with a characteristic frequency which is state-dependent. The temporal coherence $\mathcal{L}(t) = \langle S^+ \rangle$, is given by $\mathcal{L}(t) = \langle \mathcal{B}(\omega_u, t) | \mathcal{B}(\omega_d, t) \rangle$ to within a normalisation factor; averaged over bath states, it simulates the experimentally measured signal.

II. FLOQUET THEORY

Floquet’s theorem is generally applicable to periodically-forced systems, classical or quantum, but it allows one specifically to write solutions to the Schrödinger equation in terms of quasi-energy states (QES) $|\psi_l(t)\rangle = \exp(-i\epsilon_l t) |\Phi_l\rangle$ where ϵ_l is the quasi energy, $|\Phi_l(t)\rangle = |\Phi_l(t + \tau_{\text{tot}})\rangle$, τ_{tot} is the period and $l = 1, \dots, D$ (D is the dimension). However, for problems (such as our present study) where we require only “stroboscopic” knowledge of our system (i.e. read-out once every period τ_{tot}), the solution is even simpler. We can obtain Floquet phases/modes simply as the eigenvalues/eigenstates

of the one-period unitary evolution operator $\hat{T}(\tau_{\text{tot}}, 0)$. The Floquet modes $|\Phi_l\rangle$, obey the eigenvalue equation:

$$\hat{T}(\tau_{\text{tot}}) |\Phi_l\rangle = \lambda_l |\Phi_l\rangle \equiv \exp(-i\mathcal{E}_l) |\Phi_l\rangle \quad (1)$$

where now \mathcal{E}_l is the eigenphase (the Floquet phase) and $\epsilon_l = \mathcal{E}_l/\tau_{\text{tot}}$ is the quasienergy. For sensing, we can obtain Floquet phases/modes simply as the eigenvalues/eigenstates of $\hat{T}_{u,d}$, the basic periodic sequence; for example, for the CPMG sequence in Fig.2, $\tau_{\text{tot}} = 4\tau$. In that instance $\hat{T}_i |\Phi_{il}\rangle = e^{-i\mathcal{E}_l^{(i)}} |\Phi_{il}\rangle$ where $i = u, d$ denotes the state of the sensor spin. The eigenphases for $N_p = 1$ fully determine the time-evolution of the system since if the pulse sequence is repeated N_p times, we just scale the eigenphases, so for longer time-propagation:

$$\left(\hat{T}_i\right)^{N_p} |\Phi_{il}\rangle = e^{-iN_p \mathcal{E}_l^{(i)}} |\Phi_{il}\rangle. \quad (2)$$

In the present work, we show that these Floquet eigenphases and eigenstates have particular important properties:

(a) The eigenvalues are the same for the upper and lower states, i.e. $e^{i\mathcal{E}_l^{(u)}} = e^{i\mathcal{E}_l^{(d)}} \equiv e^{i\mathcal{E}_l}$. This holds even for pulses of finite duration, in typical cases. In other words, the evolution of the $\hat{T}_u^{(N_p)} \mathcal{B}(0)$ and $\hat{T}_d^{(N_p)} \mathcal{B}(0)$ are characterised by the same set of effective frequencies $\epsilon_l = \mathcal{E}_l/\tau_{\text{tot}}$, in contrast to typical static, geometric approaches where two distinct sets of frequencies ω_{ul} and ω_{dl} are involved.

(b) The eigenvectors do not, in general, coincide but we show that (to within a phase term), the eigenvectors are related to each other by a half-period evolution e.g. $\hat{T}_u(\tau_{\text{tot}}/2) |\Phi_{ul}\rangle \propto |\Phi_{dl}\rangle$.

(c) Minima in coherence (of prime importance for sensing,

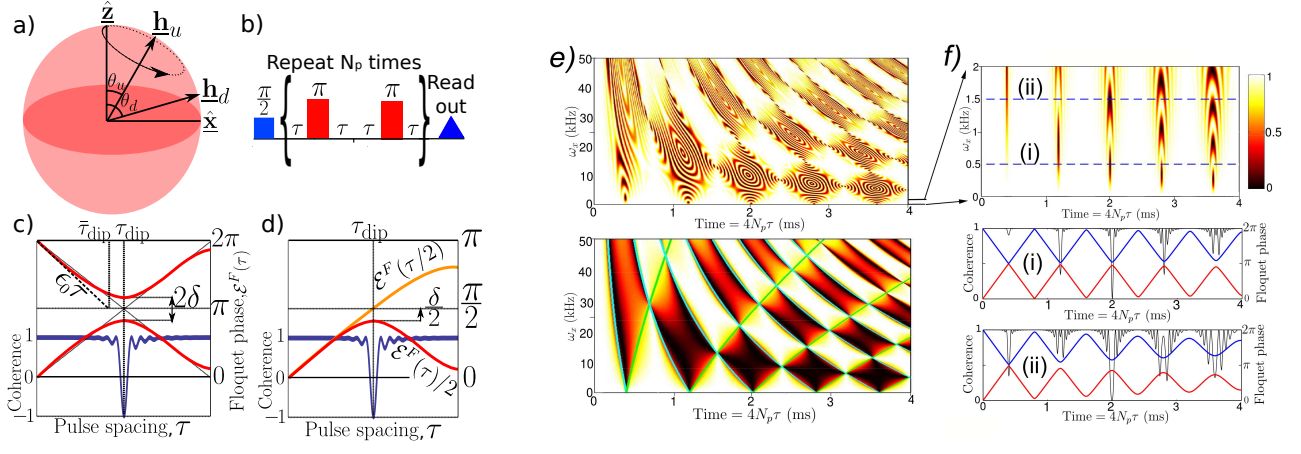


FIG. 2: **(a)** usual **Geometric** approach: under CPMG-N control **(b)** the detected spins represent two-state systems which precess about effective magnetic field, depending on the “up” $|u\rangle$ and “down” $|d\rangle$ states of the probe spin. The coherence dips are understood by following the precessions and relative angles between these spins, with increasing N . **(c)** **Spectroscopic** picture. The dips in coherence occur at avoided crossings of the Floquet eigenstates. Both the position and contrast of the decoherence dip is related to the curvature of the crossing. This is characterised by the splitting between the states 2δ and the deviation from the early $\tau \rightarrow 0$ linear evolution. The early time evolution (the ϵ_0 quasienergy) gives the the dip position $\bar{\tau}_{dip}$ for average Hamiltonian theory; the coherence minimum is given by $\mathcal{E}(\frac{\tau_{dip}}{2}) = \frac{\pi}{2}$. **(d)** The dip contrast depends on the degree of curvature of the crossing, characterised by the level-repulsion strength, $\delta = 2 \left(\frac{\mathcal{E}(\tau_{dip})}{2} - \mathcal{E}(\frac{\tau_{dip}}{2}) \right)$. **(e)** NV-center decoherence “diamonds”. While typical experimental studies scan along parallel field (ω_z) component (thus remaining in weak-coupling, single-dip regime), scanning the *transverse* magnetic field (ω_x) would produce diamond pattern of high decoherence regions, as avoided crossings widen (and even overlap) then narrow (here $\omega_z = 0$ and $A_{||} = 50\text{kHz}$). Upper panel shows full oscillating coherence function, for $N_p = 10$ pulse pairs, lower panel shows coherence envelopes, filled as $N_p \rightarrow \infty$. Here $\omega_z = 0$. Boundaries of the diamonds trace out (green) $\tau = \pi/2(\omega_d + \omega_u)$ and (cyan) $\tau = \pi/2(\omega_d - \omega_u)$ (see below). **(f)** expanded version of low field region showing shape of avoided crossings versus coherence traces corresponding to two cuts (i),(ii), indicated in the upper panel.

whether sharp dips or not) occur at avoided crossings of Floquet eigenstates, where $e^{i\mathcal{E}_l} \simeq e^{i\mathcal{E}_{l'}}$. Once the Floquet phases and modes are obtained, one can obtain the general form of the decoherence for arbitrary times which, averaged over bath states, yields:

$$\langle \mathcal{L}(t = N_p 4\tau) \rangle = \frac{1}{D} \sum_{l,l'} e^{-iN_p(\mathcal{E}_l - \mathcal{E}_{l'})} |\langle \Phi_{dl'} | \Phi_{ul} \rangle|^2 \quad (3)$$

Derivations of **(a)-(c)** are given in the Appendix. Although properties (a)-(c) are quite generic, physical insight on the Floquet picture is more easily gained from two-state systems, where direct comparison with usual geometric methods [21, 23, 24] is also possible. For the two-state case, eigenvalues must be conjugate pairs $\lambda_{\pm} = e^{\pm i\mathcal{E}}$. Level crossings occur when $\lambda_+ \simeq \lambda_-$ hence the crossings must occur at $\mathcal{E} \simeq 0, \pi, 2\pi$. The generic properties of states at avoided crossings (see Appendix) then imply coherence dips occur at $\mathcal{E} \simeq \pi$. We now first investigate the Floquet dynamics for these two-state single-spin or single pseudospin models.

A. Single spin or spin pair detection

Both pair flip-flop dynamics as well as single spin-dynamics (in systems like NV centres where a crystal field leads to non trivial one-spin dynamics) can be approximated by a two-state Hamiltonian. We term this the pseudospin

model, noting that for single-spin detection there is a genuine spin, while for pair-dynamics [14, 16] it is a pseudospin. It has led to a successful, widely used geometric model (see Fig.2(a) and [34]) where the evolution of the pseudospin is conditional on the state $i = u, d$ of the probe and corresponds to precession about an effective magnetic field: $H_i = \frac{1}{2} \mathbf{h}^i \cdot \boldsymbol{\sigma} = \frac{1}{2} (X\sigma_x + Z_i\sigma_z)$ where σ_x, σ_z are Pauli matrices in the usual spin basis; in the pseudospin case of course, we have $|\uparrow\downarrow\rangle \rightarrow |\uparrow\rangle$ and $|\downarrow\uparrow\rangle \rightarrow |\downarrow\rangle$. The X, Z_i depend on the physical system (see [34] for details); but for NV centers $\mathbf{h}^u \simeq (\omega_x, 0, A_{||} + \omega_z)$ while $\mathbf{h}^d \simeq (\omega_x, 0, \omega_z)$ where $\frac{\mu_0 \mathbf{B}_0}{\hbar} = (\omega_x, 0, \omega_z)$ is the external magnetic field, and $A_{||}$ the parallel component of the hyperfine interaction. For spin pair-sensing, on the other hand, $\mathbf{h}^i = \frac{1}{2} (C_{12}, 0, \Delta A_i)$ where $\Delta A_i = 2(A_1 - A_2) \langle i | \hat{S}_z | i \rangle$ represents the energy detuning between the nuclear spins in the pair and \hat{S} represents the operator for the sensor spin. The eigenvalues of H_i are $\omega_{u,d} = \pm \frac{1}{2} \sqrt{X^2 + Z_{u,d}^2}$ and the orientation of the effective field is $\theta_i = \arctan(X/Z_i)$. For two state systems, we obtain:

$$\langle \mathcal{L}(\tau) \rangle = 1 - 2 \left[\frac{\cos^2 [\mathcal{E}(\tau)/2] - \cos^2 [\mathcal{E}(\tau/2)]}{\cos^2 [\mathcal{E}(\tau)/2]} \right] \sin^2 [N_p \mathcal{E}(\tau)] \quad (4)$$

This is a key result of the present work as it means one can give the full coherence function using only the Floquet phases. To calculate the Floquet eigenphase $\mathcal{E}(\tau)$, as well as its half-

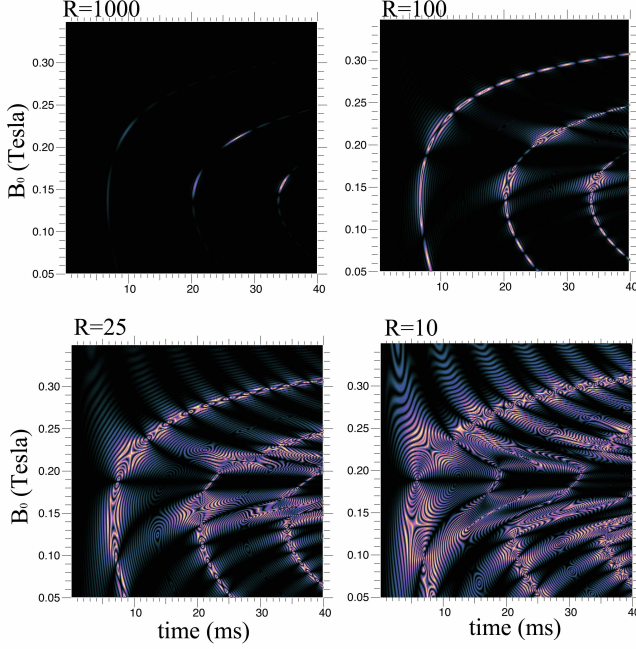


FIG. 3: Coherence decay behavior for an electron spin detecting a flip-flopping pair of nuclear spins, for a donor in silicon system (see [34]) with tunable interactions. $\mathcal{L}(B_0, t)$ exhibits a rich structure in the two-dimensional τ, B_0 plane which is not evident in the normal traces at constant B_0 . Decoherence map is shown for different $R = \Delta A/C_{12}$, ($\Delta A = A_1 - A_2$). Large R corresponds to weaker dipolar coupling C_{12} and the maps trace the locus of a set of isolated sharp dips in coherence. For smaller R , there are no longer single dips; nevertheless the envelopes (given by $F(\tau)$) are well-defined and track the behavior of the underlying Floquet avoided crossings. The background oscillatory structure depends on N_p , the envelopes do not. Time $t \equiv 4N_p\tau$; (colour scale linear, with black $\equiv 1$, yellow < 0.5). Similar behavior is obtained for several transitions of Si:Bi and other donors, but specific parameters are for $12 \rightarrow 9$ ESR transition of Si:Bi and $2N_p = 40$.

period value $\mathcal{E}(\tau/2)$ in Eq.4, one may use $\cos(\mathcal{E}(s)) = \cos(2\omega_u s) \cos(2\omega_d s) - \sin(2\omega_u s) \sin(2\omega_d s) \cos(\theta_u - \theta_d)$ with $s = \tau$ or $s = \tau/2$. Thus the coherence takes the form $\mathcal{L}(\tau) = 1 - 2F(\tau) \sin^2[N_p \mathcal{E}(\tau)]$, which is the product of a smooth envelope $F(\tau)$, independent of N_p , superimposed on a fast oscillating function $\sin^2[N_p \mathcal{E}(\tau)]$, dependent on N_p .

Full comparison with geometric methods are in [34] where we argue it is the condition

$$\mathcal{E}(\tau_{dip}/2) = \pi/2 \quad (5)$$

which best specifies the dip positions. The *depth* of the dip is related to the eigenvalue splitting parameter $\delta = \pi - \mathcal{E}(\tau_{dip})$; at the dip

$$\mathcal{L}(t = 4N_p\tau_{dip}) = 1 - 2 \sin^2(N_p\delta). \quad (6)$$

Hence, if $\mathcal{E} = \pi$, there is no dip, so a true level crossing provides no signal. For $N_p\delta \gtrsim \pi/2$ the width and shape of the dip becomes largely independent of N_p and is fully determined by the Floquet anti-crossing and envelope function,

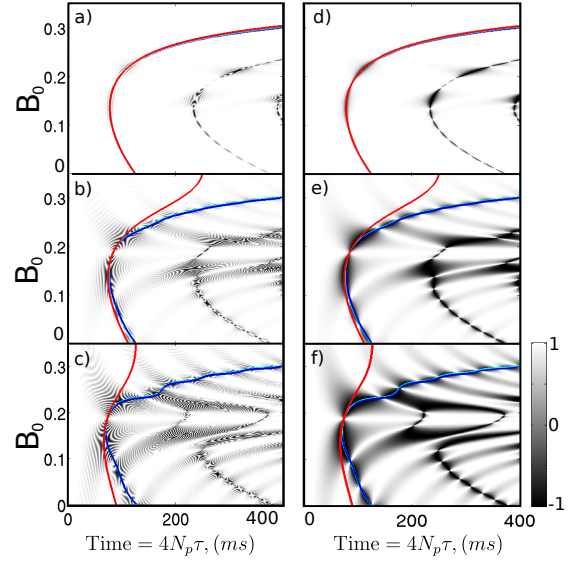


FIG. 4: Comparisons between the dip positions obtained with Eq.4 (blue line) and average Hamiltonian theory Eq.7 (red line) for the full coherence function (left panels) as well as its envelope (right). Within the field sweep there are global weak-coupling points (eg $B_0 \approx 0.19$ T) where there is weak coupling regardless of the cluster properties and where the decoherence envelope collapses into a single sharp dip, a useful feature if high resolution is required: here there is always good agreement with average Hamiltonian theory. These points correspond to so called optimal working points [30, 31] of silicon donors. Hence, the advantage of such systems as future spin sensors, in addition to their very long ~ 1 s coherence times, is that a magnetic field sweep could tune the dynamics from the weak to strong coupling regimes. (a) and (d) $R=100$ (b) and (e) $R=20$ (c) and (f) $R=10$.

since the $\sin^2(N_p\delta)$ prefactor simply superposes fast oscillations on $F(\tau)$. A narrow avoided-crossing (low splitting, δ small) gives a single, sharp (but weaker) coherence dip, while a large δ crossing has a broad envelope. It is only for low $N_p\delta \ll \pi/2$ that the dip height is strongly dependent on N_p ; here the central height increases as $(N_p\delta)^2$.

Comparison with Average Hamiltonian models (see [34] for details). A frequently used approximation in spin sensing is the average Hamiltonian model whereby the eigenvalues ω_{av} of, $\frac{1}{2}(H_u + H_d)$, the time-averaged Hamiltonian provide an estimate of the dip positions and that $T_{dip} = \frac{N_p\pi}{\omega_{av}}$. From Fig.2 (c) and (d) we can equate linear behaviour in our eigenvalues (narrow crossing, linear shape) both with the occurrence of a sharp dip as well as validity of the averaged Hamiltonian model. In particular, for small τ , $\mathcal{E}(\tau) \simeq 4\epsilon_0\tau$ corresponds to the averaged Hamiltonian results. Expanding the $\cos \mathcal{E}(\tau)$ from below Eq.4, for small τ , we easily obtain $\epsilon_0 = \frac{1}{2}(\omega_u^2 + \omega_d^2 + 2\omega_u\omega_d \cos(\theta_u - \theta_d))^{1/2}$ and thus:

$$\bar{\tau}_{dip} = \frac{\pi}{2(\omega_u^2 + \omega_d^2 + 2\omega_u\omega_d \cos(\theta_u - \theta_d))^{1/2}} \quad (7)$$

Expressing quantities in terms of the pseudofield components $X, Z_{u,d}$ we can show that this is equivalent to the expression

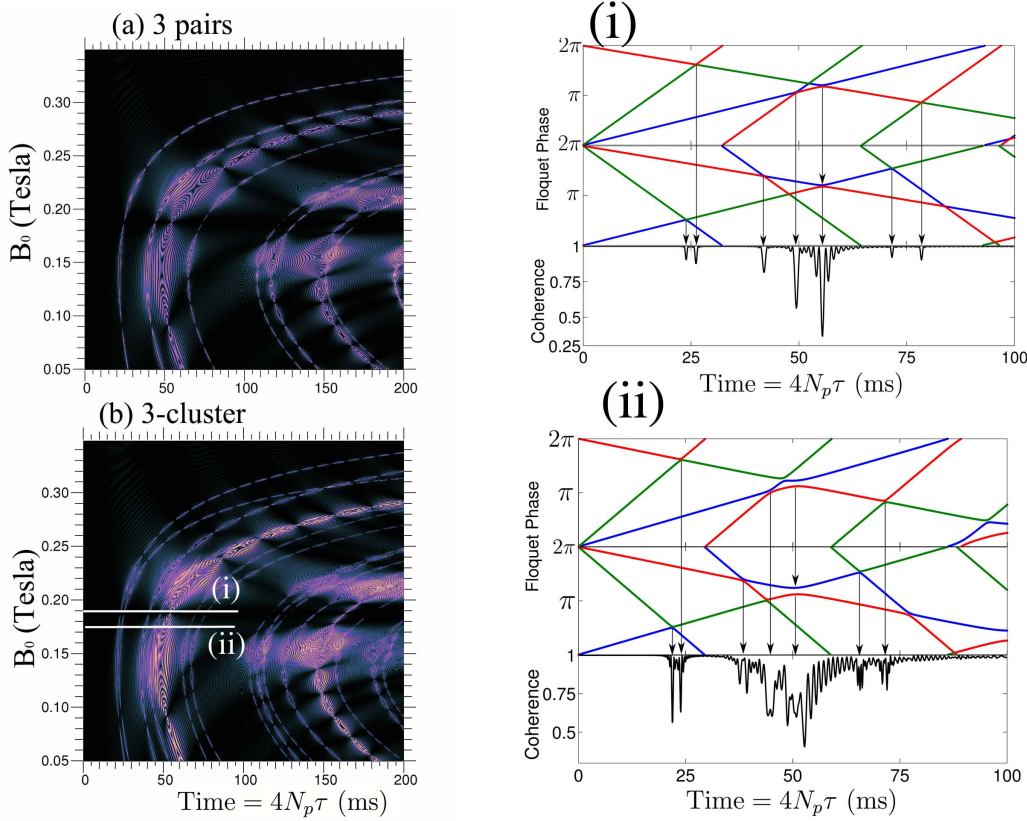


FIG. 5: Fingerprinting multiple environmental spin cluster-pairs via their decoherence “bar-codes” illustrates the effect of 3-body correlations. The figure shows the coherence as a function of magnetic field B_0 and pulse interval τ , calculated with a full numerical propagation under the total Hamiltonian for $N_p = 100$. (a) denotes three independent pairs while (b) shows three interacting spins, with otherwise equivalent dipolar couplings and intrabath interactions as illustrated in Fig.1(b). One evident difference (and signature of a cluster of three spins) are the doublets due to the two separate subspaces of the three interacting spins. The splittings are directly related to the interactions. For the 3-cluster, in fact there is a secular contribution from interactions between spins, greatly amplifying their contribution. The two right hand panels (i) and (ii) show single traces corresponding to the cuts in (b) as well as the six corresponding eigenphases: in case (i) in a weak coupling regime the dips are narrow and the eigenphases behave like three independent pairs; the eigenvalues correspond to conjugate pairs (with blue, red and green lines denoting the three pairs). In case (ii) there is stronger coupling, the avoided crossings of the corresponding eigenphases are broader giving raise to the features shown in the coherence maps.

$\omega_{av} = \frac{1}{2}((X^2 + (\frac{Z_u + Z_d}{2})^2)^{1/2}$ used in spin-detection experiments [14, 16] and to $\omega_{av} \simeq \frac{1}{2}(\omega_u + \omega_d)$ for $\theta_u \simeq \theta_d$.

III. APPLICATIONS

A. Experimental control of quasienergy crossings

The above motivates us to investigate possibilities for experimental control of the avoided crossings, by varying δ , even in the simple one-spin or spin-pair case. In typical sensing with NV-centers, we have $\omega_z \gtrsim \omega_x \gg A$, thus in Eq.7, we have $\theta_u \sim \theta_d \ll \pi$, thus $\bar{\tau}_{dip} \simeq \frac{\pi}{2(\omega_u + \omega_d)}$. However, setting $\omega_z = 0$ and increasing ω_x causes the anti-crossings to widen and narrow successively, forming a checkerboard pattern of diamonds. This behavior was illustrated in Fig.2 (e) and (f). In particular Fig.2 (e) illustrates the usefulness of the 2D map; it is not easy to clearly discern the behavior from an

individual trace (as in Fig.2 (f)) especially if N_p is not very large. We note that higher harmonics have larger δ than lower harmonics at the same parameters.

However, here we consider in addition $S = 1/2$ systems as potential sensors. These might include silicon vacancies but in particular we focus on electron donors in silicon. Although techniques analogous to optical read-out and polarization of NV centres are not fully developed, there has been considerable progress in single-spin detection [25–27]. These systems benefit also from extremely long coherence times (of order seconds) for cryogenically cooled samples. They are also an ideal test-bed for the theory as one can vary θ_u, θ_d over a wide range as magnetic field B_0 is swept. For donor systems, the surrounding ^{29}Si nuclear spin dynamics does not generate an ac signal as there is no internal crystal axis, in contrast to the case of NV centers in diamond where the surrounding nuclear spins precess around an effective quantisation axis which is no longer only the external magnetic field. For donors, sin-

gle strongly coupled ^{29}Si nuclei have recently been detected via the static shift of the donor frequency [28]. However, the interesting coherence dynamics in these systems involve only pairs or larger clusters of spins where the flip-flopping dynamics generates an ac signal [29, 30].

Formally, the state-conditional dynamics for donors is very similar to that for NV centers: The dynamics correspond to an effective spin precessing about effective magnetic fields $\mathbf{h}^i = \frac{1}{2}(C_{12}, 0, \Delta A_i)$ where $\Delta A_i = (A_1 - A_2)P_i$; But in contrast to NV centers $P_i(B_0) = 2\langle i|\hat{S}_z|i\rangle$, the polarisation of the state (see [34]) varies strongly with the magnetic field [31, 32], while for NVs, $\langle i|\hat{S}_z|i\rangle = 0, \pm 1$ is fixed for the modest fields used in experiments.

Fig.3 shows the field-dependence of the coherence for a variety of coupling strengths. The behavior may be compared with the NV-centers: in this case, the coherence dips trace out a curved locus. like NVs, for stronger $X \equiv C_{12}/2$ component of the pseudofield, the envelopes broaden, but there is a similar pattern of intermittent broadening and narrowing. There is a striking feature at $(B_0 = 188\text{mT})$ in Fig.3 where all decoherence envelopes “collapse” to a sharp dip. This is one of a set of special fields (Optimal working points) where $\theta_u \simeq \theta_d$ and $\omega_u \simeq \omega_d$ and which have been investigated theoretically and experimentally for their favourable coherence properties [30, 31, 33].

But, in the present work, we find also that these points correspond also to very narrow Floquet avoided crossings, at which $\delta \rightarrow 0$. Fig.4 compares dip position predicted by average Hamiltonian theory Eq.7 with the accurate dip condition $\mathcal{E}(\tau_{\text{dip}}/2) = \pi/2$. In Fig.4, $\Delta A = (A_1 - A_2)$, (which approximately sets the timescale for $R \gg 1$) was fixed, while C_{12} (the intra-bath dipolar coupling) was varied to obtain different values of $R = \Delta A/C_{12}$.

By means of a detailed theoretical analysis we can show that average Hamiltonian theory is valid if (i) $|\mathbf{h}_u + \mathbf{h}_d| \gg |\mathbf{h}_u - \mathbf{h}_d|$ or if (ii) $|\mathbf{h}_u - \mathbf{h}_d| \gg |\mathbf{h}_u + \mathbf{h}_d|$. Condition (i) corresponds to the weak-coupling regimes typical of NV sensing experiments, where $\omega_u \simeq \omega_d$ and $\theta_u \simeq \theta_d$; it is also the regime of the Optimal Working Points, where average Hamiltonian theory is always valid. Regime (ii) is not typical of sensing experiments; for the spin-1/2 system of Fig. 4, it would correspond to the spins nearly antialigned, thus $P_u \simeq -P_d$. For Fig. 4 condition (ii) implies $(\Delta A)^2(P_u - P_d)^2 \gg (C_{12})^2 + (\Delta A)^2(P_u + P_d)^2$. In particular, for $P_u \approx -P_d$ we obtain the condition $|\Delta A(P_u - P_d)| \gg |C_{12}|$. Noting that $|P_u - P_d| \simeq 0.2 - 2$, this means that average Hamiltonian theory is valid at all fields for large $R \gtrsim 100$ as seen in Fig. 4(a). However, for increasing intra-bath dipolar coupling C_{12} , the theory ceases to be valid away from the small OWP regime in the center, as seen in Figs. 4 (b) and (c) for smaller R .

B. Detection of multi-spin clusters

In this section we apply the Floquet approach to the system depicted in Fig.1(d): we compare the decoherence “fingerprint” of three independent spin pairs (analogous, formally, to the detection of three independent spins by NMR) with a 3-

cluster which, in the absence of many-body interactions would give a similar signature.

For the 3-cluster, we take three spins, with hyperfine couplings $A_k \equiv A_1, A_2, A_3$ to the sensor spin and with mutual dipolar interactions $C_{ij} \equiv C_{12}, C_{23}, C_{31}$. Disregarding interactions, the energy cost of the spin flips is $\Delta_{ij} = A_i - A_j$.

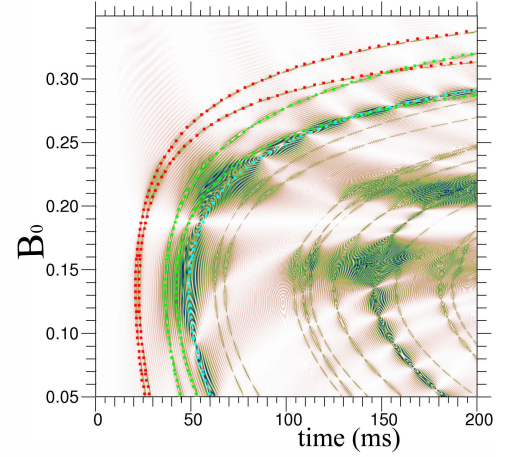


FIG. 6: Decoherence for an interacting cluster of three spins (3-cluster). The coloured lines show comparisons with Eq.10 showing excellent agreement with numerics obtained by diagonalisation of the full joint sensor-cluster Hamiltonian.

For the independent pairs, we take three spin pairs, with the same dipolar interactions C_{ij} as the 3-cluster, but which are independent of each other. To have similar frequencies as the 3-cluster, we must have similar energy cost of a all three spin flips; and they must obey the cyclic condition of the 3-cluster $\Delta_{12} + \Delta_{23} + \Delta_{31} = 0$. Pair 1 has two spins with interaction C_{12} and a pair of hyperfine couplings (A_1, A_2) ; pair 2 has interaction C_{23} and hyperfine couplings (A_2, A_3) ; pair 3 has C_{31} and hyperfine couplings (A_3, A_1) . We take $C_{12} = C_{23} = \frac{1.05}{2\pi}$ kHz and $C_{31} = \frac{2.2}{2\pi}$ kHz, realistic values for nuclear impurities in the silicon lattice. We take $A_1 = \frac{180}{2\pi}$ kHz, $A_3 = \frac{100}{2\pi}$ kHz and $A_2 = 0$, thus our pairs correspond to $R \simeq 100 - 40$ (as defined in Fig.3) so the interactions are sufficiently weak to make their detection challenging but sufficiently strong to, below, illustrate important features. The choice of $A_2 = 0$ does not involve much loss of generality. If a state-dependent Hamiltonian is chosen, the A_1, A_2, A_3 values can be shifted by an arbitrary constant without perturbing the dynamics. If the full Hamiltonian is considered, there can be higher order effects such as hyperfine mediated corrections to C_{ij} . This correction is very small for our parameters but is tested by full numerics below.

Solution of total Hamiltonian First we set aside all pseudospin approximations and do diagonalisations of the full Hamiltonian followed by time-propagation, using the complete 8-state basis of the 3-cluster as well as the complete basis of the bismuth sensor including the host nuclear spin. Thus, unlike Fig.3, we do not use the analytical form for the parameter P_i ; it emerges from the numerics. We evaluate the decoherence numerically rather than using Eq.4. A similar

calculation was carried out with the three disjoint pairs, then the decoherence was averaged over the thermal ensemble of nuclear spin states (of which there are eight for the 3-cluster). Figure 5 shows maps of the coherence in the (τ, B_0) -space in both cases.

One conclusion to be drawn from comparisons between full numerics and the analytical (one-pair) Eq.4 is that the structure in Fig.3 is surprisingly robust; without bath state averaging, full numerics give similar structure to Fig.3 (obtained from Eq.4 for one bath state).

One striking feature of the 3-cluster decoherence map in Fig.5(b) is that some lines are split into “doublets” with very similar structure. The origin of these is in the average over the bath states; examining maps for the individual 8 bath states, we see that while the $I_z = \pm 3/2$ cluster states $|\uparrow\uparrow\uparrow\rangle$ and $|\downarrow\downarrow\downarrow\rangle$ make no appreciable contribution, the doublets arise from the separate $I_z = \pm 1/2$ subspaces, which do not mix. In other words, the $|\uparrow\uparrow\downarrow\rangle, |\uparrow\downarrow\uparrow\rangle$ and $|\downarrow\uparrow\uparrow\rangle$ states with total quantum number $I^z = +1/2$ interact only weakly with the equivalent $I^z = -1/2$ subspace, but each provides a locus of dips with a slightly different shift. In contrast to the spin pairs, in the case of the 3-cluster, the secular Ising $(C_{jk}\hat{I}_{zj}\hat{I}_{zk})$ components yield a non-trivial dynamical effect.

Fig.5(i) and (ii) also shows a cut for two field values and compares with the behavior of the Floquet eigenstates. We can see that near the “weak-coupling” regime of optimal working points (i), the dips are sharp and narrow as are the avoided crossings; in contrast, away from the OWP point, avoided crossings are broader and even overlap (ii); the level splitting is much larger. We can estimate the point where two eigenvalues will collide, and hence τ_{dip} by exploiting the fact that in either case, the average Hamiltonian theory value is not too far from the accurate value $\bar{\tau}_{dip} \simeq \tau_{dip}$. We estimate Floquet quasi-energies by considering only the diagonals. We obtain:

$$\epsilon_l = \frac{1}{2}(A_i - A_j - A_k)(P_u + P_d) + C_{ij} + C_{ik} - C_{jk} \quad (8)$$

where $i, j, k \equiv 1, 2, 3$ or cyclic permutations give $\epsilon_{l=1,2,3}$ quasienergies.

Thus we estimate the dip positions from the fact that the quasi-energies represent the *gradients* of the spectral lines in Fig.5 (i) and (ii), hence estimate the degeneracy point :

$$\tau_{dip}^{(lm)} \simeq \frac{2\pi}{\epsilon_l - \epsilon_m} \quad (9)$$

for the dip arising from the difference between the l and m -th quasienergy. One finding is that the secular contribution from the dipolar coupling greatly amplifies the effect of the (usually weaker) C_{ij} dipolar coupling between the nuclei, as it is a linear contribution. This is in contrast to disjoint pairs; if the dipolar coupling is weak, since $\omega_i = \pm \frac{1}{4}\sqrt{C_{12}^2 + (P_i\Delta A)^2}$, for $C_{12} \ll P_i\Delta A$ the non-secular contributions in the disjoint pairs represent a very small quadratic shift.

In terms of the interaction strengths, the two dips of the first doublet correspond to:

$$\tau_{dip}^{(\pm 12)} \simeq \frac{2\pi}{|\Delta_{12}(P_u + P_d) \pm 2(C_{31} - C_{23})|} \quad (10)$$

and similarly for other doublets.

In Fig.6 we compare values from Eq.10 with the full numerics. Thus the mean position exposes the value of Δ_{12} while the splittings expose the dipolar coefficients.

IV. CONCLUSIONS

The extension of technologies such as MRI and NMR to the nano-scale is an outstanding technical challenge which is leading not only rapid experimental progress, but also the development of new methods to analyse data and to optimise information gathering on the atomic scale structure.

Motivated by this, in the present work we introduce Floquet spectroscopy as an insightful new paradigm for understanding and analysis of spin sensing experiments. The approach is universally valid for any type of periodic driving whether resonant or not. Hence, here potential applications have been explored for analysis of different physical regimes and sensors which are not necessarily associated with a single sharp resonant ‘dip’ but may nevertheless potentially still offer well delineated features.

Our key findings are (i) that there is an underlying structure associated with Floquet avoided crossings and the Floquet spectrum which is potentially information rich; it represents an envelope on the usually studied coherence dips with a shape controlled by the widths of the avoided crossings. (ii) that the Floquet approach clarifies also regimes where the commonly-used average Hamiltonian theory methods will fail. (iii) The method’s generality extends beyond single spin and pseudospin systems and is also useful for higher dimensional spin systems, and potentially any dynamical decoupling protocol, provided it is temporally periodic.

Acknowledgements We are very grateful to Setrak Balian, Gary Wolfowicz and Gavin Morley for helpful discussions.

Appendix A: Floquet spectrum

1. Coherence minima and avoided crossings

A key result of the present work is that the coherence dips associated with single spin sensing are associated with avoided crossings of the underlying Floquet spectrum and in this appendix, this conjecture is justified.

In our study, we consider the important class of spin-sensing experiments for which an electronic sensor spin S is coupled to each environmental nucleus via the effective Hamiltonian:

$$\hat{H} \approx \langle i | \hat{S}_z | i \rangle \mathbf{A} \cdot \mathbf{I} \quad (A1)$$

Where $i = u, d$ and \mathbf{A} is a vector representing the hyperfine interaction. The dependence on S_z only arises because of the large energy difference between electronic and nuclear states; in the case of NV-centers, the above is valid only for magnetic fields of magnitude and orientation which does not mix the

electronic states. The result is a state conditional Hamiltonian:

$$\hat{H} = \frac{1}{\sqrt{2}}[|u\rangle\langle u| \otimes H_u + |d\rangle\langle d| \otimes H_d] \quad (\text{A2})$$

where the H_i are the effective bath Hamiltonians discussed in Section II A in the main text so that an initial joint sensor-target spin state $\psi(0) \simeq \frac{1}{\sqrt{2}}(|u\rangle + |d\rangle)\mathcal{B}(0)$ evolves into an (in general) entangled state:

$$\psi(t) = \frac{1}{\sqrt{2}}(|u\rangle\mathcal{B}_u(t) + |d\rangle\mathcal{B}_d(t)). \quad (\text{A3})$$

Experiments probe the coherence $\mathcal{L}(t) = \langle S^+ \rangle$. While experimental comparison involves averaging over thermal bath states $\text{Tr}[\rho S^+]$, without loss of generality we consider a pure state $\mathcal{L} = \langle \psi(t) | S^+ | \psi(t) \rangle \propto \langle \mathcal{B}_u(t) | \mathcal{B}_d(t) \rangle$.

Maximum entanglement occurs whenever $\langle \mathcal{B}_u(t) | \mathcal{B}_d(t) \rangle = 0$. However, the general condition for a minimum or dip to be observed is in fact $|\mathcal{B}_u(t)\rangle = -|\mathcal{B}_d(t)\rangle$. This is regardless of the particular dynamical decoupling sequence applied. The key question for design of an experimental pulse sequence (say, CPMG) is for which pulse interval τ and total pulse number $N \equiv 2N_p$ will correspond to underlying quantum evolution

$$\langle \mathcal{B}_u(t = 4N_p\tau) | \mathcal{B}_d(t = 4N_p\tau) \rangle = -1 \quad (\text{A4})$$

and thus a minimum in the function \mathcal{L} , which to within an unimportant normalisation factor we take, $\mathcal{L} = \langle \mathcal{B}_u(t) | \mathcal{B}_d(t) \rangle$ (we note that for decoherence experiments probing $|\mathcal{L}|$, this in fact corresponds to a *maximum* in the coherence).

The Floquet approach is based on the premise that for any periodically driven quantum system, the Floquet states Φ_j fulfil the same role as eigenstates of a Hamiltonian in a time-independent system. Thus if the initial quantum state is projected into a Floquet basis, i.e. $\mathcal{B}(0) = \sum_l a_l \Phi_l$, then its temporal evolution is known for all time.

A central finding for the present work is that for the pulsed dynamical decoupling, the eigenspectrum is independent of the sensor spin state thus $\mathcal{E}_l^{(u)} = \mathcal{E}_l^{(d)} \equiv \mathcal{E}_l(\tau)$ where the Floquet eigenspectrum $\mathcal{E}_l(\tau)$ is a function of the experimentally chosen pulse interval τ .

The above results are proved in the next section, but we use them now to explain why coherence minima are associated with avoided crossings. Since the Floquet spectra are the same, if there is an avoided crossing and thus a near degeneracy, $e^{\mathcal{E}_l(\tau)} \simeq e^{\mathcal{E}_k(\tau)}$ in the u subspace of sensor states, there will simultaneously be an avoided crossing in the lower d subspace of sensor states.

2. Avoided crossings for two-level system

Although the eigenspectra are the same, in general the corresponding eigenstates or Floquet states are not. $\Phi_d(\tau) \neq \Phi_u(\tau)$ for arbitrary τ . Hence the temporal evolution:

$$\begin{aligned} \mathcal{B}_u(t) &= a_{u+}\Phi_{u+}e^{-iN_p\mathcal{E}(\tau)} + a_{u-}\Phi_{u-}e^{+iN_p\mathcal{E}(\tau)} \neq \\ \mathcal{B}_d(t) &= a_{d+}\Phi_{d+}e^{-iN_p\mathcal{E}(\tau)} + a_{d-}\Phi_{d-}e^{+iN_p\mathcal{E}(\tau)} \end{aligned} \quad (\text{A5})$$

and thus entanglement with the sensor is established since the sensor-target $\mathcal{B}_{u,d}(t)$ state is no longer factorisable.

One exception occurs for $\tau = 0$, where all the Floquet states reduce to the unperturbed (thermal states). For a two-state system, without loss of generality, $\Phi_{u+}(\tau = 0) = \Phi_{d+}(\tau = 0) = |\uparrow\rangle$ or alternatively $\Phi_{u-}(\tau = 0) = \Phi_{d-}(\tau = 0) = |\downarrow\rangle$.

Another, most interesting, exception is at a level crossing, where the eigenstates take the same form. It is a textbook result for level crossings (also known as Landau-Zener transitions) that the unperturbed states are maximally mixed and become sums and differences of the unperturbed states. The implication for the present case, is that the Floquet states for *both upper and lower state must* coincide at approximately $\frac{1}{\sqrt{2}}(|\downarrow\rangle \pm |\uparrow\rangle)$. This allows for two distinct possibilities:

(i) In the first case,

$$\begin{aligned} \Phi_{u+} &= \Phi_{d+} \simeq \frac{1}{\sqrt{2}}(|\downarrow\rangle + |\uparrow\rangle) \text{ and} \\ \Phi_{u-} &= \Phi_{d-} \simeq \frac{1}{\sqrt{2}}(|\downarrow\rangle - |\uparrow\rangle) \end{aligned} \quad (\text{A6})$$

This possibility is the trivial case where the Floquet states for upper and lower sensor state are identical. There is never any difference in the evolution, no entanglement and so $\langle \mathcal{B}_u(t) | \mathcal{B}_d(t) \rangle = +1$.

(ii) In the second case,

$$\begin{aligned} \Phi_{u+} &= \Phi_{d-} \simeq \frac{1}{\sqrt{2}}(|\downarrow\rangle + |\uparrow\rangle) \text{ and} \\ \Phi_{u-} &= \Phi_{d+} \simeq \frac{1}{\sqrt{2}}(|\downarrow\rangle - |\uparrow\rangle) \end{aligned} \quad (\text{A7})$$

In this case, $\langle \mathcal{B}_u | \mathcal{B}_d \rangle = \cos 2N_p\mathcal{E}(\tau)$ which may for an appropriate choice of $N_p \approx \pi/2\mathcal{E}$ attain the minimal value for a dip $\langle \mathcal{B}_u | \mathcal{B}_d \rangle = -1$.

Diagonalisation of the two dimensional unitary matrix is straightforward (see [34]) and it is clear its eigenvalues must be conjugate pairs $\lambda_{\pm} = e^{\pm i\mathcal{E}}$. For a two-level case, the avoided crossing condition is $\lambda_+ = \lambda_-$ and hence coherence dips must occur at $\mathcal{E} \simeq 0, \pi, 2\pi$ with case (i) occurring at $\mathcal{E} \simeq \pi$ and case (ii) occurring at $\mathcal{E} \simeq 0, 2\pi$.

3. Coherence minima for the general case

For a spin cluster of arbitrary size, an initial pure state can be projected into the upper or lower Floquet basis:

$$|\mathcal{B}(0)\rangle = \sum_l^D \langle \Phi_{il} | \mathcal{B}(0) \rangle |\Phi_{il}\rangle \quad (\text{A8})$$

where $|\Phi_{il}\rangle$ are Floquet eigenstates for upper ($i = u$) and lower ($i = d$) sensor state respectively and D is the dimension of the one-period unitary evolution operator. The state after a time $t = 4N_p\tau$ is then

$$|\mathcal{B}_i(t)\rangle = \sum_l^D e^{-iN_p\mathcal{E}_l} \langle \Phi_{il} | \mathcal{B}(0) \rangle |\Phi_{il}\rangle \quad (\text{A9})$$

where \mathcal{E}_l are the eigenphases.

Thus the coherence decay of the sensor spin ($\mathcal{L}(t) = \langle \mathcal{B}_l(t) | \mathcal{B}_u(t) \rangle$) is given in a Floquet basis by:

$$\mathcal{L}(t = N_p 4\tau) = \sum_{l,l'}^D e^{-iN_p(\mathcal{E}_l - \mathcal{E}_{l'})} |a_l|^2 |\langle \Phi_{dl'} | \Phi_{ul} \rangle|^2, \quad (\text{A10})$$

Here $|a_l|^2 = |\langle \Phi_{ul} | \mathcal{B}(0) \rangle|^2$.

The target spins are in fact in a thermal ensemble, which given small nuclear energy scale are all equally likely. Thus we must average over the thermal bath states and calculate $\langle \mathcal{L} \rangle = (1/D) \sum_j^D \mathcal{L}_j$, where \mathcal{L}_j is the coherence function evaluated for the bath initially in the j -th thermal bath state, $|\mathcal{B}_j(0)\rangle$. Under the thermal average we find $\sum_j \langle \Phi_{ul} | \mathcal{B}_j(0) \rangle \langle \mathcal{B}_j(0) | \Phi_{ul} \rangle = 1$. This produces Eq. 3 in the main text. While \mathcal{L} for a pure state is complex, the (in any case small) imaginary part vanishes under the bath average and we consider only the real part of \mathcal{L} .

Returning briefly to simplest case of $D = 2$, treated in the previous subsection, Eq. (A10) may be rewritten as

$$\langle \mathcal{L}(\tau) \rangle = 1 - 2|\langle \Phi_{d-} | \Phi_{u+} \rangle|^2 \sin^2 \left(N_p \frac{\mathcal{E}_1 - \mathcal{E}_2}{2} \right) \quad (\text{A11})$$

which is of the form $\mathcal{L}(\tau) = 1 - F(\tau)f(N_p, \tau)$ where $f(N_p, \tau) \in [0, 1]$ is a pulse number dependent oscillation. If we disregard the oscillation, we obtain the pulse number independent minimal bound of the coherence function given by $\mathcal{L}_{\text{env}}(\tau) = 1 - F(\tau)$, which we call the coherence *envelope*.

Even if these envelopes are not necessarily sharp “dips” (especially in strong-coupling regimes) they can correspond to sharply delineated structures (for both NV centers and donors) which should still be observable experimentally and can yield valuable information about the atomic-scale structure. We have shown above that the dips occur when $|\Phi_{u+}\rangle = |\Phi_{d-}\rangle$.

For a general bath, of arbitrary dimension D , we can rearrange Eq.(A10) using only orthonormality and completeness of the eigenstates $\sum_{k'} |\langle \Phi_{dk'} | \phi \rangle|^2 = 1$ into paired contributions.

$$\langle \mathcal{L} \rangle \equiv 1 - \sum_{l < l'} [|\langle \Phi_{dl'} | \Phi_{ul} \rangle|^2 + |\langle \Phi_{dl} | \Phi_{ul'} \rangle|^2] \times \sin^2 \left(N_p \frac{\mathcal{E}_l - \mathcal{E}_{l'}}{2} \right) \quad (\text{A12})$$

This is, again, composed of pulse number independent envelopes superimposed with pulse number dependent oscillations. For a minimum, we require the term in square brackets to be maximised; this will occur at a level crossing between a given pair of eigenstates l and l' as argued in the previous subsection. For $D > 2$, level crossings between $\mathcal{E}_l \approx \mathcal{E}_{l'}$ occur at arbitrary \mathcal{E}_l and no longer at $\mathcal{E}_{l,l'} \approx \pi$. Dips occurring at the point for which $|\langle \Phi_{dl'} | \Phi_{ul} \rangle|^2 = 1$ and $|\langle \Phi_{dl} | \Phi_{ul'} \rangle|^2 = 1$, generalises, to arbitrary dimension, the two-state orthogonality condition that $|\Phi_{u+}\rangle = |\Phi_{d-}\rangle$.

Appendix B: Symmetry of eigenphases for CPMG control

For decoupling sequences like CPMG, the Floquet phases are independent of the sensor spin state, regardless of the dimensionality of the bath states i.e. $\mathcal{E}_l^{(u)} = \mathcal{E}_l^{(d)} \equiv \mathcal{E}_l$. To

show this we first construct the basic propagator, for total period $\tau_{\text{tot}} = 4\tau$, which is to be repeated periodically:

$$\begin{aligned} \hat{T}_{(u)}^{(2)}(4\tau) &= \hat{T}_{(u)}(\tau) \hat{T}_{(d)}(\tau) \hat{T}_{(d)}(\tau) \hat{T}_{(u)}(\tau) \equiv \hat{T}_{(u)}(2\tau) \hat{T}_{(d)}(2\tau) \\ \hat{T}_{(d)}^{(2)}(4\tau) &= \hat{T}_{(d)}(\tau) \hat{T}_{(u)}(\tau) \hat{T}_{(u)}(\tau) \hat{T}_{(d)}(\tau) \equiv \hat{T}_{(d)}(2\tau) \hat{T}_{(u)}(2\tau) \end{aligned} \quad (\text{B1})$$

We can then obtain the eigenvalues for $\hat{T}_{(u)}^{(2)}$:

$$\hat{T}_{(u)}^{(2)}(4\tau) |\Phi_{ul}\rangle = \hat{T}_{(u)}(2\tau) \hat{T}_{(d)}(2\tau) |\Phi_{ul}\rangle = e^{-i\mathcal{E}_l} |\Phi_{ul}\rangle. \quad (\text{B2})$$

Here $\exp(-i\mathcal{E}_l)$ is the l th eigenvalue of $\hat{T}_{(u)}^{(2)}$. If we apply the half period operator, $\hat{T}_{(d)}(2\tau)$:

$$\hat{T}_{(d)}(2\tau) \hat{T}_{(u)}(2\tau) \hat{T}_{(d)}(2\tau) |\Phi_{ul}\rangle = e^{-i\mathcal{E}_l} \hat{T}_{(d)}(2\tau) |\Phi_{ul}\rangle, \quad (\text{B3})$$

this is equivalent to

$$\hat{T}_{(d)}^{(2)}(4\tau) \hat{T}_{(d)}(2\tau) |\Phi_{ul}\rangle = e^{-i\mathcal{E}_l} \hat{T}_{(d)}(2\tau) |\Phi_{ul}\rangle, \quad (\text{B4})$$

Thus $\exp(-i\mathcal{E}_l)$ is also an eigenvalue of $\hat{T}_{(d)}^{(2)}$. Eq.B4 implies that $\hat{T}_{(d)}(2\tau) |\Phi_{ul}\rangle$ is a eigenstate of $\hat{T}_{(d)}^{(2)}$, i.e. $\hat{T}_{(d)}(2\tau) |\Phi_{ul}\rangle \propto |\Phi_{dl}\rangle$, where the factor of proportionality is a complex phase $\exp(i\mu_{ld})$. Similarly,

$$\hat{T}_{(u)}(2\tau) |\Phi_{dl}\rangle = \exp(i\mu_{lu}) |\Phi_{ul}\rangle \quad (\text{B5})$$

for which $\mu_{ld} + \mu_{lu} = \mathcal{E}_l$. From this we see that each Floquet state $|\Phi_{ul}\rangle, |\Phi_{dl}\rangle$ is the half-period evolution of the other (up to a complex phase).

Appendix C: Pulses of finite duration

Provided the $\hat{T}_{(u,d)}^{(2)}(4\tau)$ can be decomposed into products of sub-propagators, as in Eq.C2, the π pulses do not have to be of very short duration. If we write:

$$\begin{aligned} \hat{T}_{(u)}(2\tau + 2\delta) &= \hat{T}_{(u)}(\tau) T_\pi(2\delta) \hat{T}_{(d)}(\tau) \\ \hat{T}_{(d)}(2\tau + 2\delta) &= \hat{T}_{(d)}(\tau) T_\pi(2\delta) \hat{T}_{(u)}(\tau) \end{aligned} \quad (\text{C1})$$

Then we can write the full propagator in the same form as previously:

$$\begin{aligned} \hat{T}_{(u)}^{(2)}(4\tau') &= \hat{T}_{(u)}(2\tau') \hat{T}_{(d)}(2\tau') \\ \hat{T}_{(d)}^{(2)}(4\tau') &= \hat{T}_{(d)}(2\tau') \hat{T}_{(u)}(2\tau') \end{aligned} \quad (\text{C2})$$

but with $\tau' = \tau + \delta$. Then all the above follow; the pulses of finite duration are still assumed to be π pulses but there can be some arbitrary evolution of the system during the finite interval δ , but properties such as the state independence of the Floquet phases still hold.

- [1] F. Jelezko, T. Gaebel, I. Popa, M. Domhan, A. Gruber and J. Wrachtrup, *Observation of Coherent Oscillation of a Single Nuclear Spin and Realization of a Two-Qubit Conditional Quantum Gate*, Phys. Rev. Lett. **93** 130501 (2004).
- [2] L. Childress, M. V. Gurudev Dutt, J. M. Taylor, A. S. Zibrov, F. Jelezko, J. Wrachtrup, P. R. Hemmer, and M. D. Lukin, *Coherent Dynamics of Coupled Electron and Nuclear Spin Qubits in Diamond*, Science **314**, 218 (2006).
- [3] J. R. Maze, P. L. Stanwix, J. S. Hodges, S. Hong, J. M. Taylor, P. Cappellaro, L. Jiang, M. V. Gurudev Dutt, E. Togan, A. S. Zibrov, A. Yacoby, R. L. Walsworth and M. D. Lukin *Nanoscale magnetic sensing with an individual electronic spin in diamond* Nature **455**, 644-647 (2008).
- [4] G. Balasubramanian, I. Y. Chan, Roman Kolesov, Mohannad Al-Hmoud, Julia Tisler, Chang Shin, Changdong Kim, Aleksander Wojcik, Philip R. Hemmer, Anke Krueger, Tobias Hanke, Alfred Leitenstorfer, Rudolf Bratschitsch, Fedor Jelezko and Jrg Wrachtrup *Nanoscale imaging magnetometry with diamond spins under ambient conditions* Nature **455**, 648-651 (2008)
- [5] T. Muller, C. Hepp, B. Pingault, E. Neu, S. Gsell, M. Schreck, H. Sternschulte, D. Steinmler-Nethl, C. Becher and M. Atature, *Optical signatures of silicon-vacancy spins in diamond*, Nature Comm. **5**, 3328 (2014).
- [6] J. Hansom, C. H. H. Schulte, C. Le Gall, C. Matthiesen, E. Clarke, M. Hugues, J. M. Taylor and M. Atature, *Environment-assisted quantum control of a solid-state spin via coherent dark states*, Nature Physics **10**, 725-730 (2014).
- [7] P. Cappellaro, L. Jiang, J. S. Hodges and M. D. Lukin, *Coherence and Control of Quantum Registers Based on Electronic Spin in a Nuclear Spin Bath*, Phys. Rev. Lett. **102**, 210502 (2009).
- [8] P. Neumann, R. Kolesov B. Naydenov, J. Beck, F. Rempp, M. Steiner, V. Jacques, G. Balasubramanian, M. L. Markham, D. J. Twitchen, S. Pezzagna, J. Meijer, J. Twamley, F. Jelezko & J. Wrachtrup, *Quantum register based on coupled electron spins in a room-temperature solid*, Nature Physics **6**, 249 (2010).
- [9] N. Bar-Gill, L. M. Pham, A. Jarmola, D. Budker and R. L. Walsworth, *Solid-state electronic spin coherence time approaching one second*, Nature Commun. **4**, 1743 (2013).
- [10] T. H. Taminiau, J. Cramer, T. van der Sar, V. V. Dobrovitski and R. Hanson, *Universal control and error correction in multi-qubit spin registers in diamond*, Nature Nano. **9**, 171176 (2014).
- [11] H. Bernien, B. Hensen, W. Pfaff, G. Koolstra, M. S. Blok, L. Robledo, T. H. Taminiau, M. Markham, D. J. Twitchen, L. Childress and R. Hanson, *Heralded entanglement between solid-state qubits separated by three metres*, Nature **497**, 86-90 (2013).
- [12] J. Cai, F. Jelezko, M. B. Plenio and A. Retzker, *Diamond-based single-molecule magnetic resonance spectroscopy*, New Journal of Physics, **15**, 013020 (2013).
- [13] C. Miller, X. Kong, J.-M. Cai, K. Melentijevi, A. Stacey, M. Markham, D. Twitchen, J. Isoya, S. Pezzagna, J. Meijer, J. F. Du, M. B. Plenio, B. Naydenov, L. P. McGuinness, and F. Jelezko *Nuclear magnetic resonance spectroscopy with single spin sensitivity* Nature Commun. **5** 4703 (2014).
- [14] Zhao, N., Hu, J. L., Ho, S. W., Wan, J. T. K. and Liu, R. B, *Atomic-scale magnetometry of distant nuclear spin clusters via nitrogen-vacancy spin in diamond*, Nature Nanotech. **6**, 242-246 (2011).
- [15] N. Zhao, J. Honert, B. Schmid, M. Klas, J. Isoya, M. Markham, D. Twitchen, F. Jelezko, R.-B. Liu, H. Fedder and J. Wrachtrup, *Sensing single remote nuclear spins*, Nature Nano. **7**, 657-662 (2012).
- [16] Fazhan Shi, Xi Kong, Pengfei Wang, Fei Kong, Nan Zhao, Ren-Bao Liu and Jiangfeng Du, *Sensing and atomic-scale structure analysis of single nuclear-spin clusters in diamond*, Nature Physics **10**, 21-25 (2014).
- [17] M. Loretz, J.M. Boss, T. Rosskopf, H.J. Mamin, D. Rugar, and C.L. Degen, *Spurious Harmonic Response of Multipulse Quantum Sensing Sequences*, Phys. Rev. X **5**, 021009 (2015).
- [18] R. Schirhagl, K. Chang, M. Loretz, and C. L. Degen, *Nitrogen-Vacancy Centers in Diamond: Nanoscale Sensors for Physics and Biology*, Ann. Rev. Chem. Phys. **65**, 83-105 (2014).
- [19] J.H. Shirley, *Solution of the Schrödinger Equation with a Hamiltonian Periodic in Time*, Phys. Rev. **138**, B979 (1965).
- [20] A. Schmidt and S. Vega J. Chem. Phys. **96**, 2655 (1992); T.O. Levante, M. Baldus, B.H. Meier and R.R. Ernst, Mol. Phys. **86** 1195 (1995). A. Schweiger and G Jeschke, *Principles of Pulse Electron Paramagnetic Resonance*, Oxford University Press, UK, 2001.
- [21] S. Kolkowitz, Q. P. Unterreithmeier, S. D. Bennett and M. D. Lukin, *Sensing Distant Nuclear Spins with a Single Electron Spin*, Phys. Rev. Lett. **109**, 137601 (2012).
- [22] TH Taminiau, JJT Wagenaar, T van der Sar, F Jelezko, VV Dobrovitski and R Hanson, *Detection and control of individual nuclear spins using a weakly coupled electron spin*, Phys. Rev. Lett. **109**, 137602 (2012).
- [23] N. Zhao, S. W. Ho, and R. B. Liu, *Decoherence and dynamical decoupling control of nitrogen vacancy center electron spins in nuclear spin baths*, Phys. Rev. B **85**, 115303 (2012).
- [24] A. Ajoy, U. Bissbort, M. D. Lukin, *Atomic-Scale Nuclear Spin Imaging Using Quantum-Assisted Sensors in Diamond*, R. L. Walsworth and P. Cappellaro, Phys. Rev. X **5**, 011001 (2015).
- [25] A. A. Morello, J. J. Pla, F. A. Zwanenburg, K. W. Chan, K. Y. Tan, H. Huebl, M. Möttönen, C. D. Nugroho, Changyi Yang, J. A. van Donkelaar, A. D. C. Alves, D. N. Jamieson, C. C. Escott, L. C. L. Hollenberg, R. G. Clark and A. S. Dzurak, *Single-shot readout of an electron spin in silicon*, Nature **467**, 687 (2010).
- [26] Pla J J, Tan K Y, Dehollain J P, Lim W H, Morton J J L, Jamieson D N, Dzurak A S and Morello A, *High-fidelity readout and control of a nuclear spin qubit in silicon*, Nature **496**, 334-38 (2013).
- [27] J. T. Muhonen, J. P. Dehollain, A. Laucht, F. E. Hudson, T. Sekiguchi, K. M. Itoh, D. N. Jamieson, J. C. McCallum, A. S. Dzurak and A. Morello, *Storing quantum information for 30 seconds in a nanoelectronic device*, Nature Nano. **9**, 986 (2014).
- [28] Jarryd J. Pla, Fahd A. Mohiyaddin, Kuan Y. Tan, Juan P. Dehollain, Rajib Rahman, Gerhard Klimeck, David N. Jamieson, Andrew S. Dzurak, and Andrea Morello *Coherent Control of a Single Si29 Nuclear Spin Qubit* Phys. Rev. Lett. **113**, 246801 (2014).
- [29] R.-B. Liu, W. Yao and L. J. Sham, New J. Phys. **9** 226 (2007); W. Yao, R.-B. Liu, and L. J. Sham, *Restoring Coherence Lost to a Slow Interacting Mesoscopic Spin Bath*, Phys. Rev. Lett. **98**, 077602 (2007).
- [30] S. J. Balian, G. Wolfowicz, J. J. L. Morton and T. S. Monteiro, *Quantum-bath-driven decoherence of mixed spin systems*, Phys. Rev. B **89**, 045403 (2014).
- [31] M. H. Mohammady, G. W. Morley and T. S. Monteiro, *Bismuth Qubits in Silicon: The Role of EPR Cancellation Resonances*,

- Phys. Rev. Lett. **105**, 067602 (2010).
- [32] G. W. Morley, P. Lueders, M. H. Mohammady, S. J. Balian, G. Aepli, C. W. M. Kay, W. M. Witzel, G. Jeschke and T. S. Monteiro, *Quantum control of hybrid nuclearelectronic qubits*, Nature Mater. **12**, 103-107 (2013).
- [33] G. Wolfowicz, A. M. Tyryshkin, R. E. George, H. Riemann, N. V. Abrosimov, P. Becker, H.-J. Pohl, M. L. W. Thewalt, S. A. Lyon and J. J. L. Morton, *Atomic clock transitions in silicon-based spin qubits*, Nature Nano. **8**, 561 (2013).
- [34] See Supplementary information.